WADC TECHNICAL REPORT 54-196

THE EFFECT OF AN AXIALLY SYMMETRIC FUSELAGE ON THE NONSTATIONARY SUPERSONIC AIRLOADS ACTING ON A WING WITH SUPERSONIC EDGES

MELVIN EPSTEIN, 1ST LT, USAF

AIRCRAFT LABORATORY

MAY 1954

WRIGHT AIR DEVELOPMENT CENTER

AF-WP-(B)-O-30 AUG 54 75

WADC TECHNICAL REPORT 54-196

THE EFFECT OF AN AXIALLY SYMMETRIC FUSELAGE ON THE NONSTATIONARY SUPERSONIC AIRLOADS ACTING ON A WING WITH SUPERSONIC EDGES

Melvin Epstein, 1st Lt, USAF

Aircraft Laboratory

May 1954

RDO No. 459-36R

Wright Air Development Center
Air Research and Development Command
United States Air Force
Wright-Patterson Air Force Base, Ohio

FOREWORD

This report was prepared by the Dynamics Branch, Aircraft Laboratory, Directorate of Laboratories, Wright Air Development Center under RDO No. 459-36R, "Theoretical Supersonic Flutter Studies". The work was done under the supervision of Mr. I. N. Spielberg, Chief, Analysis Section, Dynamics Branch.

ABSTRACT

An approximate method has been devised for determining the nonstationary air-loads on an elastic wing with supersonic edges upon which is mounted an axially symmetric body. The flow field due to an oscillating axially symmetric body isolated in a supersonic stream is superimposed on the flow field due to an oscillating elastic wing with supersonic edges. An additional velocity potential satisfying the basic linearized differential equation of fluid motion is constructed so that the required boundary conditions are satisfied on the wing. The result is a modification of the original source strength distribution on the isolated wing. This modified source strength distribution is calculated by means of a numerical integration procedure. The nonstationary air-loads for the wing may then be calculated as in Reference 1.

PUBLICATION REVIEW

This report has been reviewed and is approved:

FOR THE COMMANDER:

S H Schwartz

for D.D. McKee
Col., USAF
Chief, Aircraft Laboratory
Directorate of Laboratories

TABLE OF CONTENTS

LIST OF ILLUSTRATIONS

LIST OF ILLUSTRATIONS (Continued)

LIST OF SYMBOLS

a	distance from nose of fuselage to leading edge of wing root chord
b	root semi-chord
A_i, B_i	defined by equations (34) through (38)
c	free stream velocity of sound
D	area within fore Mach cone emanating from point (x,y)
h	amplitude of vertical displacement
h_x, h_y	dimensions of box in stream and span directions respectively
I_1, I_2	defined by equations (28) and (29) or (30) and (31)
k	reduced frequency ($= \frac{\omega b}{V}$)
L	total lift
L_i, M_i	components of lift and moment defined by equations (59), (60), (63) and (64)
$L_h, L_\alpha, M_h, M_\alpha$	components of lift and moment defined by equations (67) through (70)
M	Mach number; total moment
P	$\sqrt{(x-\xi)^2-\beta^2 y^2}$; $z=0$, or $\sqrt{(x-\xi)^2-\beta^2 r^2}$ when $z \neq 0$
q	generalized coordinate
r, θ	polar coordinates with respect to axis of body of revolution
R	$\sqrt{(x-\xi)^2-\beta^2(y-\eta)^2}$
$S(\xi)$	frontal area of body at station ξ

LIST OF SYMBOLS (Continued)

t	time
V	free stream velocity
w	downwash velocity
x,y,z	Cartesian coordinates
y_s	spanwise ordinate of strip s
x_o	location of axis of rotation
α	instantaneous angle of attack
β	$\sqrt{M^2 - 1}$
δ	change in phase angle of aerodynamic force or moment vector due to addition of body
ξ, η	coordinates of point of disturbance
ρ	free stream density
φ	velocity potential
Φ	function defined by equation 20
Ψ_b	function defined by equation 17
ω	frequency of oscillation
$\bar{\omega}$	frequency parameter ($= \frac{\omega M_2}{c\beta}$)

Subscripts and Superscripts

b	body
c	centroid of box
d	correcting
I	imaginary part

LIST OF SYMBOLS (Continued)

j	denotes box boundary
m	mid-point of segment of body axis
R	real part
s	denotes strip
T	due to translation
w	wing
α	due to instantaneous angle of attack
LE	leading edge
TE	trailing edge
	primes indicate differentiation with respect to ξ

INTRODUCTION

The trend in recent high speed airplane and missile designs has been toward low aspect ratio lifting surfaces mounted on bodies whose diameters are large fractions of the total lifting surface span. In the case of higher aspect ratio configurations, it is common practice for flutter analysts to ignore the presence of the body or to assume that the wing continues uninterrupted to the center line of the body when calculating unsteady air-load distributions on the wing. For moderate aspect ratios, flutter analysts sometimes treat the body as an infinite reflecting plane. As the aspect ratio is still further reduced so that the body diameter becomes proportionately larger, one is led to ask whether the effect of wing-body interference can still be ignored in computing non-stationary air-loads. Certainly, sufficient evidence is not available to show that such effects are unimportant. It has already been shown that the presence of a body near a low aspect ratio lifting surface in a steady compressible flow appreciably affects the load distribution of the lifting surface. (See, for example, Reference 2). One is therefore inclined to suspect that wing-body interference in non-stationary flow is likewise not negligible. Because large body diameter-wing span ratio configurations are most often encountered in high speed aircraft and missile designs, it seems appropriate to confine consideration to the case of supersonic flow.

Since the linearized problem of an isolated wing oscillating in a supersonic stream has not yet been solved exactly, it cannot be expected that an exact solution for the non-stationary supersonic wing-body problem can be obtained at this time. However, in what follows, an approximate method will be derived for determining the effect of an axially symmetric fuselage on the air-loads acting on an elastic wing with supersonic edges mounted on the body in the plane of the body diameter.

The problem of the body alone oscillating in a supersonic stream is treated in Reference 3. Recently, a group at Republic Aviation Corporation has developed an approximate method for computing oscillating air-loads on an isolated wing, all of whose edges are supersonic (Reference 1). The method can be applied to an elastic wing undergoing arbitrary, harmonic distortions. The formulation of the present problem is based on the assumptions that (a) the perturbations from a uniform flow are sufficiently small so that the flow equations may be linearized, and (b) the flow field around the wing is adequately described by a linear superposition of the velocity potential due to the wing alone, the velocity potential due to the body alone, and an additional velocity potential, which when added to the first two, causes the boundary conditions on the wing to be satisfied. The velocity potential due to the wing alone

will be taken from the work of Garrick (Reference 4), the potential for the body alone from (Reference 3); the wing-body interference potential is developed herein. The method of Reference 1 is used to obtain numerical solutions of the equations.

SECTION I

CONSTRUCTION OF THE SOLUTION

The velocity potential for the nonstationary flow over a wing with supersonic edges has been derived (under the assumption of linearized theory) in Reference 4. In that derivation, it was assumed that the actual wing may be replaced by a distribution of sources and sinks in the plane z = 0. It was shown that the strength of a source at any point on the wing is proportional to the downwash (w_w) at that point. Thus for harmonic oscillations, the velocity potential at a point (x, y) of the wing for the flow around the wing alone may be written as

$$\varphi_w(x,y,t) = -\frac{e^{i\omega t}}{\pi} \iint_D \frac{w_w(\xi,\eta) e^{-i\bar{\omega}(x-\xi)} \cos\left(\frac{\bar{\omega}}{M} R\right)}{R} \, d\xi \, d\eta \qquad (1)$$

where $\bar{\omega}$ is the frequency parameter defined as

$$\bar{\omega} \equiv \frac{\omega M}{c \beta^2} \qquad (2)$$

ω is the frequency of oscillation, M is the free stream Mach number, c is the free stream speed of sound, β is the Prandtl-Glauert factor

$$\beta = \sqrt{M^2 - 1} \qquad (3)$$

R may be written as

$$R = \sqrt{(x-\xi)^2 - \beta^2 (y-\eta)^2} \qquad (4)$$

and D is the area within the fore Mach cone emanating from the point (x, y).

The velocity potential for the nonstationary flow about a slender body of revolution has been derived (under the assumptions of linearized theory) in Reference 3. In this derivation it was assumed that the body may be replaced by a distribution of doublets along the axis of the body. The doublet intensity distribution was determined by satisfying the condition of no normal velocity at the surface of the body. It was thereby found that the doublet intensity at any point is proportional to the product of the body cross-sectional area(S) at that

point times the vertical velocity of the body axis (w_b) at the same point. Thus for harmonic oscillations, the velocity potential at any point in space for the flow around the body alone may be written (in cylindrical coordinates, (see Figure 1) as

$$\varphi_b(x,r,\theta,t) = -\frac{e^{i\omega t}}{\pi}\cos\theta\left\{\frac{\bar{\omega}}{rM}\int_0^{x-\beta r} w_b(\xi)S(\xi)e^{-i\bar{\omega}(x-\xi)}\sin\left(\frac{\bar{\omega}}{M}\rho\right)d\xi\right.$$

$$+\frac{1}{r}\int_0^{x-\beta r}\frac{[w_b(\xi)S'(\xi)+w_b'(\xi)S(\xi)](x-\xi)e^{-i\bar{\omega}(x-\xi)}\cos\left(\frac{\bar{\omega}}{M}\rho\right)}{\rho}d\xi \qquad (5)$$

$$\left.+\frac{i\bar{\omega}}{r}\int_0^{x-\beta r}\frac{w_b(\xi)S(\xi)(x-\xi)e^{-i\bar{\omega}(x-\xi)}\cos\left(\frac{\bar{\omega}}{M}\rho\right)}{\rho}d\xi\right\}$$

where a prime denotes differentiation with respect to ξ and

$$\rho \equiv \sqrt{(x-\xi)^2-\beta^2r^2} \qquad (6)$$

It is now assumed that the total velocity potential φ for the wing-body combination may be expressed as the sum of these two potentials plus a correction potential φ_d which will cause the boundary condition to be satisfied on the surface of the wing; that is:

$$\varphi = \varphi_w + \varphi_b + \varphi_d \qquad (7)$$

The boundary condition on the wing is

$$\left.\frac{\partial\varphi}{\partial z}\right|_{z=0} = \left.\frac{\partial\varphi_w}{\partial z}\right|_{z=0} + \left.\frac{\partial\varphi_b}{\partial z}\right|_{z=0} + \left.\frac{\partial\varphi_d}{\partial z}\right|_{z=0} = w_w \qquad (8)$$

However,

$$\left.\frac{\partial\varphi_w}{\partial z}\right|_{z=0} = w_w \qquad (9)$$

Since the velocity potential for the wing alone already satisfies the boundary condition for the motion of the wing, it is only necessary that

φ_d be of a form such that the vertical velocity that it induces at a given point on the wing just cancels the downwash induced by the body at the same point; that is,

$$\left.\frac{\partial \varphi_d}{\partial z}\right|_{z=0} = -\left.\frac{\partial \varphi_b}{\partial z}\right|_{z=0} \tag{10}$$

An alternate formulation of this problem is to assume that the downwash produced by the sources representing the wing must be modified to account for the downwash induced by the body so that the boundary condition on the wing is satisfied. An examination of equation (5) shows that φ_b is always zero in the plane $z = 0$ ($\theta = \frac{\pi}{2}, -\frac{\pi}{2}$). Therefore, the potential for the flow over the wing in combination with the body is of the same form as the potential for the wing alone, but the source strength distribution is modified to account for the downwash due to the body. Thus,

$$\varphi(x,y,t) = -\frac{e^{i\omega t}}{\pi}\iint_D \left[w_w(\xi,\eta) - \frac{\partial \varphi_b}{\partial z}(\xi,\eta)\right]\frac{e^{-i\bar{\omega}(x-\xi)}\cos\left(\frac{\bar{\omega}}{M}R\right)}{R}\,d\xi\,d\eta \tag{11}$$

This formulation will be used in the subsequent development.

Since φ_b is expressed in cylindrical coordinates and it is required to evaluate $\frac{\partial \varphi_b}{\partial z}$ at $z = 0$, $\frac{\partial \varphi_b}{\partial z}$ is written as follows:

$$\left.\frac{\partial \varphi_b}{\partial z}\right|_{z=0} = \left.\frac{\partial \varphi_b}{\partial r}\frac{\partial r}{\partial z}\right|_{z=0} + \left.\frac{\partial \varphi_b}{\partial \theta}\frac{\partial \theta}{\partial z}\right|_{z=0} \tag{12}$$

Noting that

$$r^2 = y^2 + z^2 \quad 1) \tag{13}$$

$$\left.\frac{\partial r}{\partial z}\right|_{z=0} = \left.\frac{z}{r}\right|_{z=0} = 0 \tag{14}$$

Since $\partial\varphi_b/\partial r$ remains finite on the wing, the first term of equation (12) vanishes. Similarly,

$$\theta = \tan^{-1}\frac{y}{z} \tag{15}$$

1) This assumption restricts consideration to only symmetrical wing-body configuration; i.e., where the axis of the body lies in the plane of the wing.

and

$$\frac{\partial \theta}{\partial z} = -\frac{y}{z^2+y^2}\bigg|_{z=0} = -\frac{1}{y} \tag{16}$$

Inspection of equation (5) shows that a function $\psi_b(x, r, t)$ may be introduced such that

$$\varphi_b(x, r, \theta, t) = \cos\theta\,[\psi_b(x, r, t)] \tag{17}$$

and therefore

$$\frac{\partial \varphi_b}{\partial \theta} = -\sin\theta\,[\psi_b(x, r, t)] \tag{18}$$

At $z = 0$, $\theta = \frac{\pi}{2}$, and $r = y$; hence,

$$\frac{\partial \varphi_b}{\partial \theta} = -\psi_b(x, y, t) \tag{19}$$

and

$$\frac{\partial \varphi_b}{\partial z}\bigg|_{z=0} = \frac{1}{y}\psi_b(x, y, t) = \frac{1}{\pi y}\Phi(x, y)e^{i\omega t} \tag{20}$$

where

$$\begin{aligned}\Phi(x,y) = &-\frac{\bar{\omega}}{yM}\int_0^{x-\beta y}\omega_b(\xi)S(\xi)e^{-i\bar{\omega}(x-\xi)}\sin\left(\frac{\bar{\omega}}{M}P\right)d\xi \\ &-\frac{1}{y}\int_0^{x-\beta y}\frac{[\omega_b(\xi)S'(\xi)+\omega_b'(\xi)S(\xi)](x-\xi)e^{-i\bar{\omega}(x-\xi)}\cos\left(\frac{\bar{\omega}}{M}P\right)}{P}d\xi \\ &-\frac{i\bar{\omega}}{y}\int_0^{x-\beta y}\frac{\omega_b(\xi)S(\xi)(x-\xi)e^{-i\bar{\omega}(x-\xi)}\cos\left(\frac{\bar{\omega}}{M}P\right)}{P}d\xi\end{aligned} \tag{21}$$

and P is now

$$P = \sqrt{(x-\xi)^2-\beta^2y^2} \tag{22}$$

Substituting equation (20), (21) and (22) into equation (11) gives the complete expression for the potential at point (x,y) on the wing of the wing-body combination. The pressure jump at this point is then obtained from the potential as

$$p = -2\rho\left(\frac{\partial \varphi}{\partial t} + V\frac{\partial \varphi}{\partial x}\right) \tag{23}$$

The lift (positive down) on a streamwise strip of the wing is given by

$$L_s = -\int_s p\,dx \tag{24}$$

and the stalling moment about a spanwise axis, x_o, is

$$M_s = -\int_s p(x-x_o)\,dx \tag{25}$$

SECTION II

METHOD OF APPLICATION

Up to the present time, completely analytical evaluations of integrals of the form of equations (1) and (21) have not been accomplished. For rigid body motions, equation (1) has been approximately evaluated by expanding the integrand in powers of $\bar{\omega}$ as in Reference 5. On the other hand, equation (1) has been approximately evaluated even for the case of arbitrary wing elastic deformation modes in Reference 1 by means of a numerical integration technique. In this paper, both of these methods will be combined to evaluate equation (21). The results of this evaluation may then be used directly in calculating the nonsteady air-loads acting on the wing of the wing-body combination.

The first step in this technique is to subdivide the wing into a number of small rectangular boxes of dimensions h_x and h_y, as shown in Figure 1. Boxes along the wing trailing edge are made half-size in the stream direction, in accordance with the procedure of Reference 1. The body is also divided into sections, the chordwise dimensions of which are made equal to the chordwise dimension of the wing boxes, h_x. The size of the boxes is not important from the theoretical point of view, as long as they do not become too large in the stream direction. However, certain ratios of length to width of the rectangle are more advantageous for computing purposes. (For a more detailed discussion of box size see Reference 1).

The essence of the method of Reference 1 is that, by making the boxes small enough, the downwash over any box can be considered as essentially constant and it can be removed from within the integral of equation (1). Then by expanding the numerator of the remaining integrand in a power series in $\bar{\omega}$, retaining as many terms as are required for accuracy in practical problems, and using a mean value theorem where the power series expansion is not needed, the double integral can be evaluated for all boxes within the region of integration. This procedure will be adopted for the evaluation of equation (21).

EVALUATION OF THE BODY-INDUCED DOWNWASH

If, then, the grid of boxes is made fine enough, it is reasonable to assume that w_b and S are constant along each segment into which the body axis has been divided. Then, the values of w_b and S and their derivatives with respect to ξ at any point

along a segment are taken to be the values at the center of the segment. Equation (21) then becomes

$$\Phi(x,y) = -\sum_j{}' \left\{ \frac{\bar{\omega} w_{b_j} S_j}{\gamma M} \int^{\beta_j} e^{-i\bar{\omega}(x-\xi)} \sin\left(\frac{\bar{\omega}}{M} P\right) d\xi \right. \tag{26}$$
$$\left. + \left(\frac{w_{b_j} S_j' + w_{b_j}' S_j + i\bar{\omega} w_{b_j} S_j}{\gamma} \right) \int^{\beta_j} \frac{(x-\xi) e^{-i\bar{\omega}(x-\xi)}}{P} \cos\left(\frac{\bar{\omega}}{M} P\right) d\xi \right\}$$

where the symbol $\sum_j{}'$ stands for summation over those segments of the fuselage centerline included within the fore Mach cone emanating from the point (x, y) on the wing, and the symbol $\int^{\beta_j}$ stands for integration in the x direction over the length of each of these segments. For a body section whose center line is cut by the fore Mach cone, the integration is performed only up to the Mach line. Thus equation (26) may be written as follows:

$$\Phi(x,y) = -\sum_j{}' \left\{ \frac{\bar{\omega} w_{b_j} S_j}{\gamma M} I_{1_j} + \left(\frac{w_{b_j} S_j' + w_{b_j}' S_j + i\bar{\omega} w_{b_j} S_j}{\gamma} \right) I_{2_j} \right\} \tag{27}$$

For the case of segments wherein the body axis is not cut by the fore Mach cone,

$$I_{1_j} = \int_{x_{j-1}}^{x_j} e^{-i\bar{\omega}(x-\xi)} \sin\left(\frac{\bar{\omega}}{M} P\right) d\xi \tag{28}$$

and

$$I_{2_j} = \int_{x_{j-1}}^{x_j} \frac{(x-\xi) e^{-i\bar{\omega}(x-\xi)}}{P} \cos\left(\frac{\bar{\omega}}{M} P\right) d\xi \tag{29}$$

where $x_j - x_{j-1} = h_x$. For the case of the segment wherein the body axis is cut by the fore Mach line,

$$I_{1_j} = \int_{x_{j-1}}^{x-\beta y} e^{-i\bar{\omega}(x-\xi)} \sin\left(\frac{\bar{\omega}}{M} P\right) d\xi \tag{30}$$

and

$$I_{2_j} = \int_{x_{j-1}}^{x-\beta y} \frac{(x-\xi) e^{-i\bar{\omega}(x-\xi)} \cos\left(\frac{\bar{\omega}}{M} P\right)}{P} \, d\xi \tag{31}$$

The integrals defined by equations (28), (29), (30), and (31) may be evaluated as follows. For those body segments which are within one and a half box lengths in the flow direction from the point (x,y), (i.e., $(x - x_{j-1}) \leq 3/2\, h_x$) , the integrands in these integrals may be expanded in powers of $\bar{\omega}$. Formulas are presented below for the values of these integrals wherein the integrands were expanded to the second power of $\bar{\omega}$. These formulas should provide engineering accuracy for most problems. Should increased accuracy be desired, it can be achieved by using these formulas with a very fine grid, or a coarse grid and more accurate formulas which include higher powers of $\bar{\omega}$. Thus for a "near" body segment not cut by a Mach line,

$$I_1 = A_1 \bar{\omega} + A_2 \bar{\omega}^2 \tag{32}$$

$$I_2 = B_0 + B_1 \bar{\omega} + B_2 \bar{\omega}^2 \tag{33}$$

where

$$A_1 = \frac{1}{2M}\left[(x-x_{j-1})\sqrt{(x-x_{j-1})^2-\beta^2y^2} - \beta^2 y^2 \cosh^{-1}\frac{(x-x_{j-1})}{\beta y}\right.$$
$$\left. -(x-x_j)\sqrt{(x-x_j)^2-\beta^2y^2} + \beta^2 y^2 \cosh^{-1}\frac{(x-x_j)}{\beta y}\right] \tag{34}$$

$$A_2 = \frac{i}{3M}\left\{\left[(x-x_j)^2-\beta^2y^2\right]^{3/2} - \left[(x-x_{j-1})^2-\beta^2y^2\right]^{3/2}\right\} \tag{35}$$

$$B_0 = \sqrt{(x-x_{j-1})^2-\beta^2y^2} - \sqrt{(x-x_j)^2-\beta^2y^2} \tag{36}$$

$$B_1 = \frac{i}{2}\left[(x-x_j)\sqrt{(x-x_j)^2-\beta^2y^2} + \beta^2y^2\cosh^{-1}\frac{(x-x_j)}{\beta y}\right.$$

$$\left. -(x-x_{j-1})\sqrt{(x-x_{j-1})^2-\beta^2y^2} - \beta^2y^2\cosh^{-1}\frac{(x-x_{j-1})}{\beta y}\right] \qquad (37)$$

$$B_2 = \frac{1}{6M^2}\left\{(1+M^2)\left[(x-x_j)^2-\beta^2y^2\right]^{3/2} - (1+M^2)\left[(x-x_{j-1})^2-\beta^2y^2\right]^{3/2}\right.$$

$$\left. +3\beta^2M^2y^2\left[\sqrt{(x-x_j)^2-\beta^2y^2} - \sqrt{(x-x_{j-1})^2-\beta^2y^2}\right]\right\} \qquad (38)$$

Formulas for I_1 and I_2 for the case of "near" segments wherein the body axis is cut by the Mach line can be obtained from the above formulas by putting $x_j = x - \beta y$.

For body segments which are more than one and a half box lengths removed from the wing point (x,y), $(x - x_j \geq 3/2\ h_x)$, the exponential and trigonometric terms of the integrands of equations (28), (29), (30) and (31) vary very slowly over the length of the segment provided h_x is reasonably small. Hence, good approximations to the values of these integrals may be obtained by considering these terms as constant and equal to their values at the mid-point of the segment over which the integration is being performed, and then integrating the remaining part of the integrand directly. That is, it is assumed for "far" segments that

$$I_1 \approx e^{-i\bar{\omega}(x-\xi_m)}\sin\left[\frac{\bar{\omega}}{M}P(\xi_m)\right]\int d\xi \qquad (39)$$

and

$$I_2 \approx e^{-i\bar{\omega}(x-\xi_m)}\cos\left[\frac{\bar{\omega}}{M}P(\xi_m)\right]\int \frac{(x-\xi)}{P(\xi)}\,d\xi \qquad (40)$$

where

$$\xi_m = \frac{x_j + x_{j-1}}{2} \qquad (41)$$

For those body segments wherein the body center line is not cut by a Mach line, these integrals can be shown to have the values

$$I_1 = e^{-i\bar{\omega}(x-\xi_m)} \sin\left[\frac{\bar{\omega}}{M} P(\xi_m)\right](x_j - x_{j-1}) \qquad (42)$$

and

$$I_2 = e^{-i\bar{\omega}(x-\xi_m)} \cos\left[\frac{\bar{\omega}}{M} P(\xi_m)\right]\left[\sqrt{(x-x_{j-1})^2 - \beta^2 y^2} - \sqrt{(x-x_j)^2 - \beta^2 y^2}\right] \qquad (43)$$

For those body segments wherein the body center line is cut by a Mach line, the same equations can be used with $x_j = x - \beta y$.

These equations make it possible to calculate the increments in downwash on the wing due to the body. It should be noted that these incremental downwash velocities have components both in phase and out of phase with the wing motion.

DETERMINATION OF THE NONSTATIONARY LIFT AND MOMENT DISTRIBUTIONS

The application of the method described in the previous sections to the calculation of the unsteady air-loads on the wing of a wing-body combination will now be described. Although the method is generally applicable to an elastic wing experiencing harmonic oscillations of arbitrary mode shape, for simplicity the following derivation will be restricted to a wing-body configuration undergoing rigid-body symmetrical motions. In order to determine the potential at a point (x,y) on the wing, equation (11) must be evaluated over the region of integration D bounded by the forward Mach cone emanating from (x,y), the wing leading edges, and the sides of the body. The boxes on the wing which contribute to φ (x,y,t) are indicated by the cross-hatched area in Figure 2. In keeping with the assumptions made previously, the downwash over a box will be considered constant and equal to its value at the center of the box. Thus the geometrical downwash due to the motion of the wing is

$$w_w(\xi_c, \eta_c) = i\omega[q_1 + (\xi_c - x_0)q_2] + Vq_2 \qquad (44)$$

where q_1 and q_2 are the generalized coordinates in the vertical translation and pitching modes respectively; (ξ_c, η_c) are the coordinates of the centroid of the box on the wing, and x_o is the location of the pitch axis.

The downwash at (ξ_c, η_c) induced by the body must now be determined. A Mach forecone is drawn from (ξ_c, η_c); those body segments included within this cone (as shown in Figure 2) will contribute to the induced downwash at this point.

The geometrical downwash at any point along the body center line can be written in terms of the generalized coordinates as follows:

$$w_b = i\omega[q_1 + (\xi - x_o) q_2] + V q_2$$

From this one can immediately write:

$$w_{bj} = w_b(\xi_{mj}) = i\omega[q_1 + (\xi_{mj} - x_o) q_2] + V q_2 \qquad (45)$$

$$w_{bj}' = i\omega q_2 \qquad (46)$$

where ξ_{mj} is the coordinate of the center of the jth body segment and is defined by equation (41).

Using the above expressions for the geometrical downwash of the body, one can rewrite equations (20) and (27) as follows (dropping the $e^{i\omega t}$ terms for convenience)

$$\left[\frac{\partial \varphi_b}{\partial z}(\xi_c, \eta_c)\right]_{z=0} = \frac{1}{\pi \eta_c} \bar{\Phi}(\xi_c, \eta_c)$$
$$= -i\omega q_1 \bar{\Phi}_{1h} - i\omega q_2 \bar{\Phi}_{2h} - V q_2 \bar{\Phi}_{2\alpha} - i\omega q_2 \bar{\Phi}_{2h}' \qquad (47)$$

where

$$\bar{\Phi}_{1h} = \frac{1}{\pi \eta_c^2} \sum_j{}' \left(\frac{\bar{\omega}}{M} S_j I_{1j} + i\bar{\omega} S_j I_{2j} + S_j' I_{2j}\right) \qquad (48)$$

$$\bar{\Phi}_{2h} = \frac{1}{\pi \eta_c^2} \sum_j{}' \left(\frac{\bar{\omega}}{M} S_j I_{1j} + i\bar{\omega} S_j I_{2j} + S_j' I_{2j}\right)(\xi_{mj} - x_o) \qquad (49)$$

$$\bar{\Phi}_{2\alpha} = \bar{\Phi}_{1h} \qquad (50)$$

$$\bar{F}_{2h'} = \frac{1}{\pi \eta_c^2} \sum_j' S_j I_{2j} \tag{51}$$

Thus, the total downwash which enters into equation (11) is

$$w_w(\xi_c, \eta_c) - \left[\frac{\partial \varphi}{\partial z}(\xi_c, \eta_c)\right]_{z=0}$$
$$= i\omega q_1 \left[1 + \bar{F}_{1h}\right] + i\omega q_2 \left[(\xi_c - x_0) + \bar{F}_{2h} + \bar{F}_{2h'}\right] + V q_2 \left[1 + \bar{F}_{2\alpha}\right] \tag{52}$$

Equation (11) can be evaluated in accordance with the "box" method of Reference 1, leading to the following general form for the velocity potential at point (x,y), which is now assumed to be at the center of box "i":

$$\varphi(x,y) = \varphi_i$$
$$= \left[i\omega \sum_j' \varphi_{ij} h_j^{(1)}\right] q_1 + \left[i\omega \sum_j' \varphi_{ij} h_j^{(2)} + V \sum_j' \varphi_{ij} \alpha_j^{(2)}\right] q_2 \tag{53}$$

where

φ_{ij} = the potential at the center of box i due to a constant unit downwash velocity at box j,

$$h_j^{(1)} = 1 + \bar{F}_{1hj} \tag{54}$$

$$h_j^{(2)} = (\xi_{cj} - x_0) + \bar{F}_{2hj} + \bar{F}_{2h'j} \tag{55}$$

$$\alpha_j^{(2)} = 1 + \bar{F}_{2\alpha j} \tag{56}$$

$\sum_j'$ denotes summation over all boxes included within the region of integration D, defined previously. Using equations (23) and (24), together with the assumption that the potential at the center of a box can be considered as the mean value over the entire box, Reference 1 shows that the downward load acting on a chordwise strip of the wing is given by

$$L = 2\rho i\omega \sum_{LE}^{TE} \varphi_i \Delta x_i + 2\rho V \varphi_{TE} \tag{57}$$

where the index i ranges over all boxes in the strip from leading edge (LE) to trailing edge (TE) and φ_{TE} is the value of the potential at the trailing edge of the strip. Δx_i is the dimension of box i in the stream direction. Substituting equation (53) into equation (57) and non-dimensionalizing yields the following expressions for the non-stationary sectional lift coefficients:

$$\frac{L}{-4\rho b V^2 k^2} = (L_1 + iL_2)\frac{g_1}{b} + (L_3 + iL_4)g_2 \tag{58}$$

where

$$L_1 + iL_2 = \frac{1}{2b^2}\sum_i \Delta x_i \sum_j{}' \varphi_{ij} h_j^{(1)} - \frac{i}{2bk}\sum_j{}' \varphi_{TE,j} h_j^{(1)} \tag{59}$$

$$L_3 + iL_4 = \frac{1}{2b^3}\sum_i \Delta x_i \sum_j{}' \varphi_{ij} h_j^{(2)} - \frac{i}{2b^2 k}\sum_j{}' \varphi_{TE,j} h_j^{(2)}$$
$$- \frac{i}{2b^2 k}\sum_i \Delta x_i \sum_j{}' \varphi_{ij} \alpha_j^{(2)} - \frac{1}{2bk^2}\sum_j{}' \varphi_{TE,j} \alpha_j^{(2)} \tag{60}$$

with $k = \frac{b\omega}{V}$, the local reduced frequency, at the wing root.

In a similar manner, using equations (25), a general expression for the pitching moment on a strip about the axis of pitch x_o and equations for the moment coefficients are obtained.

$$M = -x_o L + 2\rho i\omega \sum_i \varphi_i x_i \Delta x_i + 2\rho V x_{TE} \varphi_{TE} - 2\rho V \sum_i \varphi_i \Delta x_i \tag{61}$$

$$\frac{M}{-4\rho b^2 V^2 k^2} = (M_1 + iM_2)\frac{g_1}{b} + (M_3 + iM_4)g_2 \tag{62}$$

$$M_1 + iM_2 = -\frac{x_o}{b}(L_1 + iL_2) + \frac{1}{2b^3}\sum_i x_i \Delta x_i \sum_j{}' \varphi_{ij} h_j^{(1)}$$
$$- i\frac{x_{TE}}{2b^2 k}\sum_j{}' \varphi_{TE,j} h_j^{(1)} + \frac{i}{2b^2 k}\sum_i \Delta x_i \sum_j{}' \varphi_{ij} h_j^{(1)} \tag{63}$$

$$M_3 + i M_4 = -\frac{x_0}{b}(L_3 + iL_4) + \frac{1}{2b^4}\sum_i x_i \Delta x_i \sum_j{}' \varphi_{ij} h_j^{(2)}$$

$$-i\frac{x_{TE}}{2b^3 k}\sum_j{}' \varphi_{TE,j} h_j^{(2)} + \frac{i}{2b^3 k}\sum_i \Delta x_i \sum_j{}' \varphi_{ij} h_j^{(2)}$$

$$-\frac{i}{2b^3 k}\sum_i x_i \Delta x_i \sum_j{}' \varphi_{ij} \alpha_j^{(2)} - \frac{x_{TE}}{2b^2 k^2}\sum_j{}' \varphi_{TE,j} \alpha_j^{(2)} \qquad (64)$$

$$+\frac{1}{2b^2 k^2}\sum_i \Delta x_i \sum_j{}' \varphi_{ij} \alpha_j^{(2)}$$

SECTION III

APPLICATION TO A SPECIFIC PROBLEM

The application of the method described in the previous sections to the calculation of the unsteady air-loads on the wing of a wing-body combination will now be illustrated. Since the purpose of this example will be merely to illustrate the application of the method and to determine the order of magnitude of the effect of the body on the wing air-loads, a very coarse grid will be used in order to shorten the computations. Rigid body translation and pitching motions will be assumed so that the results may be compared with previously obtained results for the wing alone. Calculations will be done for both the wing alone and for the wing-body combination so that the effect of the body can be determined directly. The wing-alone configuration will consist of one wing of the wing-body combination reflected about the wing root chord line. The wing planform chosen is the same as the one that was used in References 1 and 5. This will also allow a comparison to be made between the results obtained with a coarse grid (7 boxes; Figure 2) and the fine grid used in Reference 1 for the wing alone case (28 boxes; Figure 1).

Since the calculations will be done for only one Mach number, it will be convenient to let the sides of the rectangles be in the ratio,

$$\frac{h_x}{h_y} = \beta \quad , \tag{65}$$

where h_x and h_y are box lengths in the x and y directions respectively. The geometry of the network, therefore, is such that the body axis is cut by a Mach line only at the boundary of a body segment.

The following parameters are used in this analysis:

$$b = \frac{1}{2}, \qquad M^2 = 1.75, \qquad \frac{\omega b}{V} = k = .04$$

$$\bar{\omega} = \frac{\omega M}{c\beta^2} = \frac{2b\omega M^2}{V\beta^2} = \frac{2kM^2}{\beta^2} = .18667$$

$$x_o = 2.25$$

$$a = 1.75$$

$\frac{\text{Maximum body diameter}}{\text{Maximum wing span}} = .25$

Wing leading edge sweep angle = 30°

The equation for the radius of the body is taken to be

$$y = .49487x - .053863x^3 \qquad (66)$$

In this example the lift and moment of the wing are calculated for unit values of $\frac{q_r}{b}$ and q_α.

A detailed drawing of the wing and body with the grid of boxes superimposed is shown in Figure 2.

The value of the potential for boxes close to the wing leading edge is obtained by weighting the result obtained for the whole box in accordance with the percentage of area of the whole box that is contained between the fore Mach cone and the leading edge.

1)

The results of calculations using equations (57) through (64) for the example described above are summarized in Figures 3 through 12.

1) After the calculations described herein were completed, the authors of Reference 1 devised a scheme whereby the lift and moment could be calculated somewhat more simply using pressure coefficients rather than velocity potentials. Since the principles involved are the same, the calculations are presented here in terms of potentials.

SECTION IV

DISCUSSION OF RESULTS

Formulas have been derived to determine the effect of the fuselage of a wing-body combination on the air-loads acting on a wing in nonstationary purely supersonic flow. The equations do not readily lend themselves to analytic evaluation. However, a procedure has been presented which allows a numerical solution of the problem.

Examination of equation (5) or (21) leads to the conclusion that the most accurate results are obtained when the ratio of body diameter to wing span is large (providing that the body fineness ratio is large so that linearized theory applies). This is deduced from the fact that the downwash induced by the body has a $1/r$ type singularity at the body axis. When the body diameter is large, no point on the wing is very close to the body axis and hence the mathematical singularity which does not actually exist physically need not be dealt with. Practically, the presence of a singularity at the body axis is not really a deterrent to the use of this method since corrections for the presence of the body are probably not required when the body diameter is small compared to the wing span, and also because accuracy is more important in the region of the wing tips than near the body.

The wing lift and moment due to harmonic rigid body translation and pitching about the mid-point of the root chord for the configuration shown in Figure 2 are presented in Figures 3 through 10. Curves of the variation of the unsteady aerodynamic coefficients along the span are presented. Curves for the wing alone are drawn for the results of References 1 and 5 and for the results of this paper. The curves for the wing-body combination are also drawn on the same graphs for comparison.

It is interesting to note that excellent agreement between lift curves is found for the wing alone case over the inboard half of the span. The lack of agreement near the tip is caused partly because of the small number of boxes in this region and partly because the calculations for some of the coefficients entail working with small differences of large numbers. The wing-alone moment curves are in good agreement over the inboard half of the wing for some of the coefficients, although the agreement is poor in other cases. This is to be expected since the moment coefficients depend on the distribution of pressures rather than total forces as in the case of the lift coefficients and accurate pressure distributions cannot be expected from the coarse grid used in these calculations.

The changes in total lifts and moments are not as extreme as may be expected from an inspection of Figures 3 through 10. Large changes do occur in the real components of the force and moment vectors due to translatory oscillations. However, since these real components are small compared to the imaginary components, the total changes in lift and moment magnitude are essentially those due to the changes of the imaginary components.

The overall effect of the body on the wing can be seen more clearly in Figures 11 and 12. The ratios of the magnitudes of the aerodynamic coefficients for the wing-body combination to the wing alone coefficients are presented in Figure 11. In this figure, the following definitions apply.

$$L_h = \sqrt{L_1^2 + L_2^2} \tag{67}$$

$$L_\alpha = \sqrt{L_3^2 + L_4^2} \tag{68}$$

$$M_h = \sqrt{M_1^2 + M_2^2} \tag{69}$$

$$M_\alpha = \sqrt{M_3^2 + M_4^2} \tag{70}$$

It is seen that the lift coefficients are affected most in the middle region of the wing (the dashed portions of the curves indicate extrapolated data), whereas the moment coefficients are altered most near the wing-body intersection. An interesting observation is that the curves for the outboard half of the semi-span are almost exactly the same for all four coefficients. The equations derived in this paper are too complex to determine whether this is the general case or whether it is only a coincidence for this particular set of parameters.

Figure 12 presents curves showing the variation of the change in phase angle of the aerodynamic vectors along the wing span. It is seen that for all coefficients, the body produces almost no phase change over the outboard two-thirds of the wing. The lift coefficients suffer very little phase change near the root, whereas an extremely large phase change takes place near the root, for the moment coefficients. The size of the phase shift may be considerably in error. As explained previously, accurate pressure distributions cannot be expected when a very coarse grid is used. Inspection of Figure 2 shows that the local chord of the lattice representing the wing changes from two to three boxes at just about the same spanwise station that the sudden change in phase shift occurs. Actually

the effect of the change in chord is not as great as the above statement might imply because the potential contributed by each box is weighted according to the percentage area of the box covered by the wing. It should be noted however that the large changes in the moment coefficient magnitudes and phase angles near the wing-body intersection may be grossly exaggerated. The singularity at the body axis causes the velocities induced by the body at points very close to th body axis to be much too large, thereby exaggerating the effect of the body on the wing air-loads in this region.

An effect which is not evident from the equations presented in the previous sections was noticed during the calculations. It was found that one of the most dominant terms involved in the calculation of the body-induced downwash was the term involving S'. Not only was this term larger than the others but it was noticed that if this term were omitted, the body-induced downwash would be of an entirely different order of magnitude and possibly even of a different sign. Thus if a circular cylinder were used as a fuselage, the results would be quite different. It seems likely, therefore, that the effects of the body on the wing air-loads are quite sensitive to body shape and the position of the wing on the body. The results of this example should therefore not be considered to be typical. However, they do show that wing-body interference effects can be significant.

SECTION V

SUMMARY AND CONCLUSIONS

An approximate method has been developed for taking into account the effect of a fuselage on the unsteady air-loads on an elastic wing with supersonic edges. A numerical procedure for obtaining solutions is presented, based on the technique employed in Reference 1 wherein the wing alone case is considered.

The results of sample calculations show that a body with maximum diameter equal to twenty-five percent of the maximum wing span appreciably affects the magnitude of the unsteady aerodynamic forces and moments, whereas the phase angles of the aerodynamic force and moment vectors are only slightly affected.

It became apparent, during the course of the sample calculations, that downwash induced on the wing by the body is very sensitive to the shape of the body. Therefore the results obtained in the sample calculations should not necessarily be considered as representative of the general effect of a body on the unsteady air-loads on a wing.

Although the example calculated herein was concerned with the effect of a body on the airloads of a wing with supersonic edges, the method is also applicable to a wing with subsonic edges, since the essence of the method is merely the modification of the downwash in the area perturbed by the wing.

REFERENCES

1. Liban, E., Neuringer, J., and Rabinowitz, S. "The Flutter Analysis of an Elastic Wing with Supersonic Edges" Republic Aviation Corporation Report No. E-SAF-1.

2. Lagerstrom, P. A. and Graham, M. E. "Remarks on Low-Aspect-Ratio Configurations in Supersonic Flow",. J.A.S., Vol. 18, No. 2, February 1951.

3. Dorrance, W. H., "Nonsteady Supersonic Flow About Pointed Bodies of Revolution". J.A.S., Vol. 18, No. 8, August 1951.

4. Garrick, I. E., and Rubinow, S. I., "Theoretical Study of Air Forces on an Oscillating or Steady Thin Wing in a Supersonic Main Stream.", NACA TN 1383, July 1947.

5. Nelson, H. C., "Lift and Moment on Oscillating Triangular and Related Wings with Supersonic Edges". NACA TN 2494, September 1951.

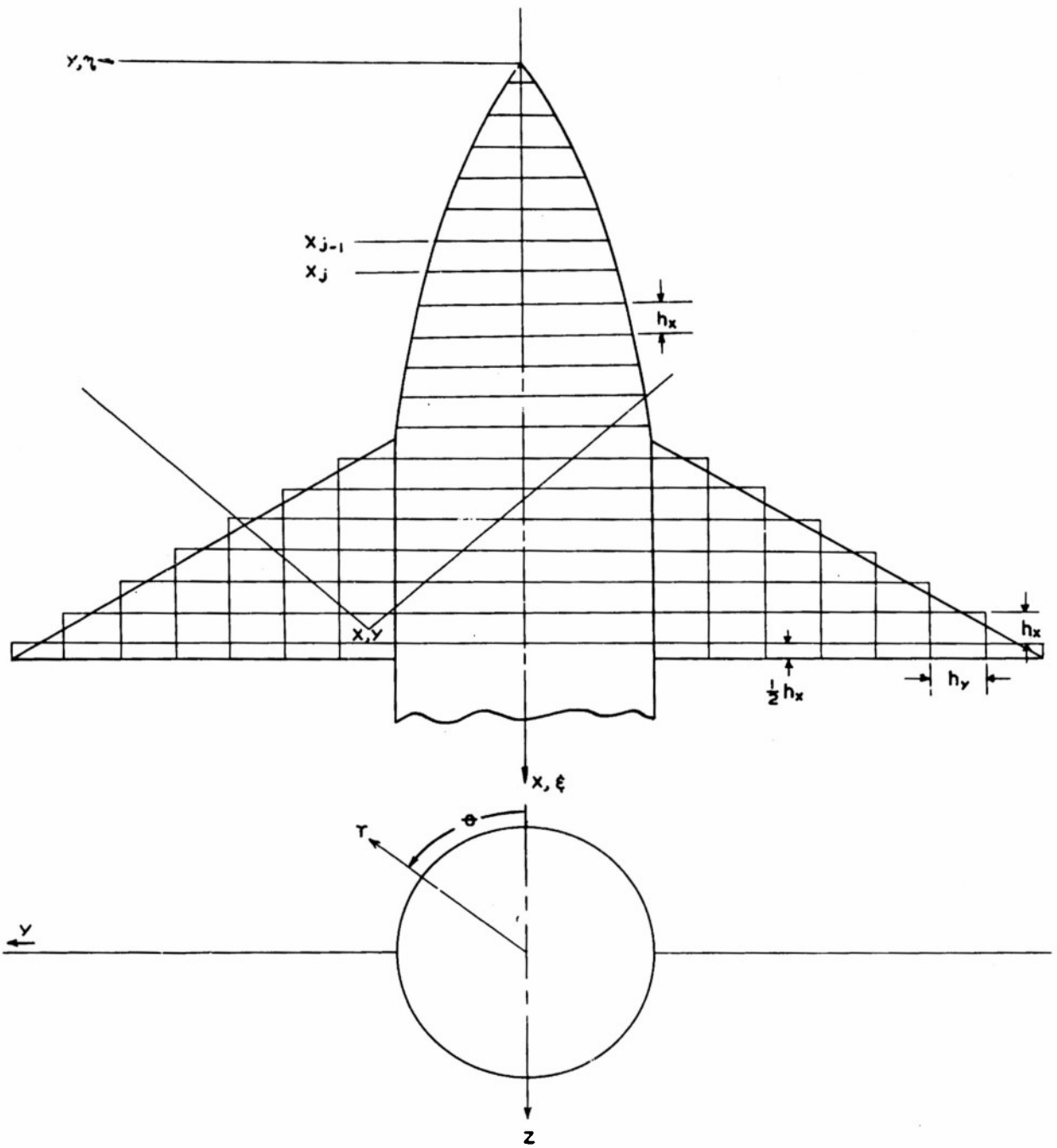

FIGURE I. COORDINATE SYSTEM AND DETAILS OF GRID SYSTEM

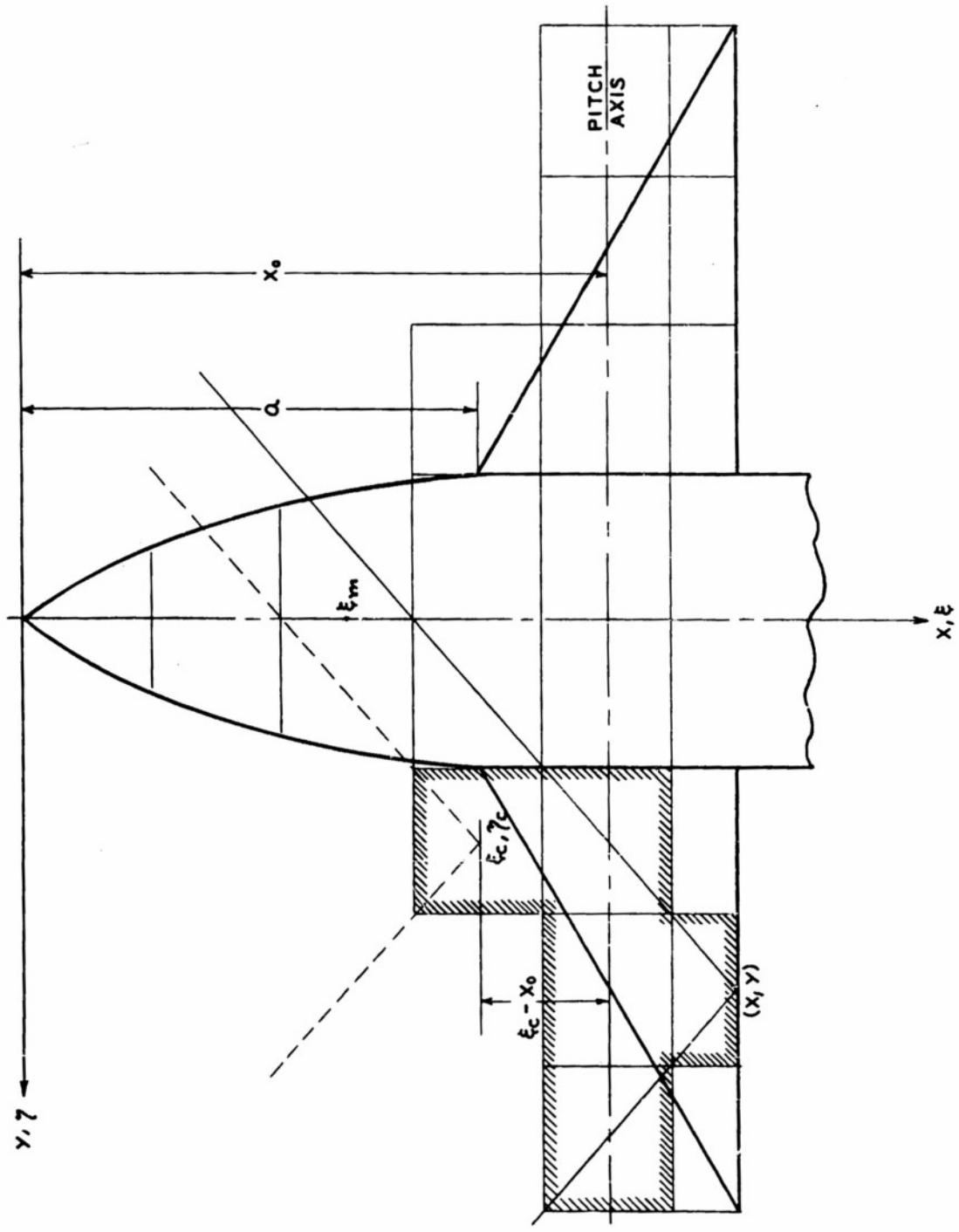

FIGURE 2. CONFIGURATION FOR ILLUSTRATIVE EXAMPLE

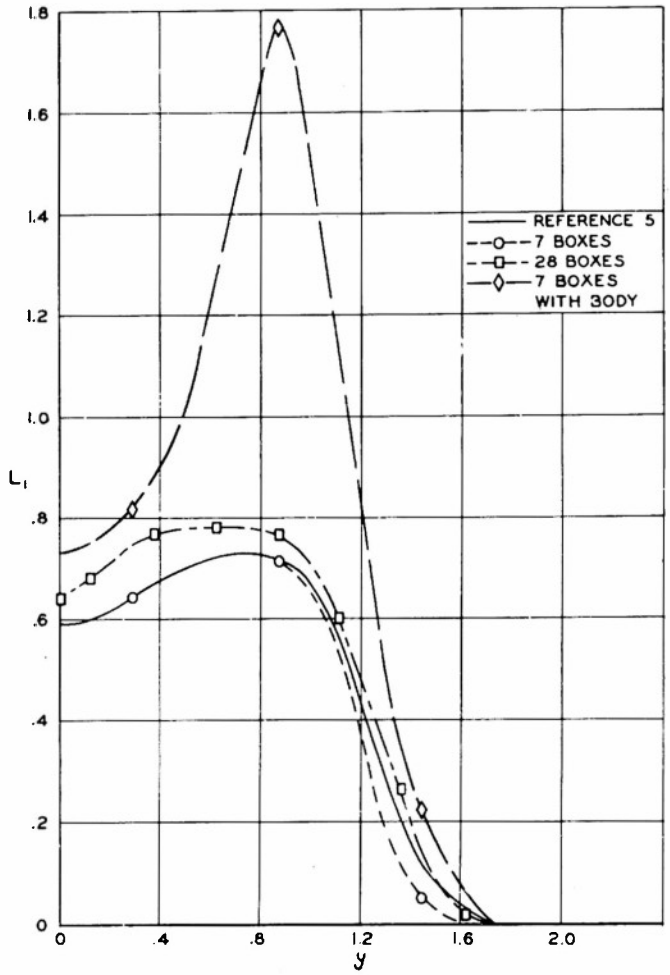

FIGURE 3. SPANWISE VARIATION OF REAL PART OF LIFT DUE TO TRANSLATION, L_1

$x_0 = 2.25$, $M^2 = 1.75$ $K = .04$ DIAMETER = .25 SPAN

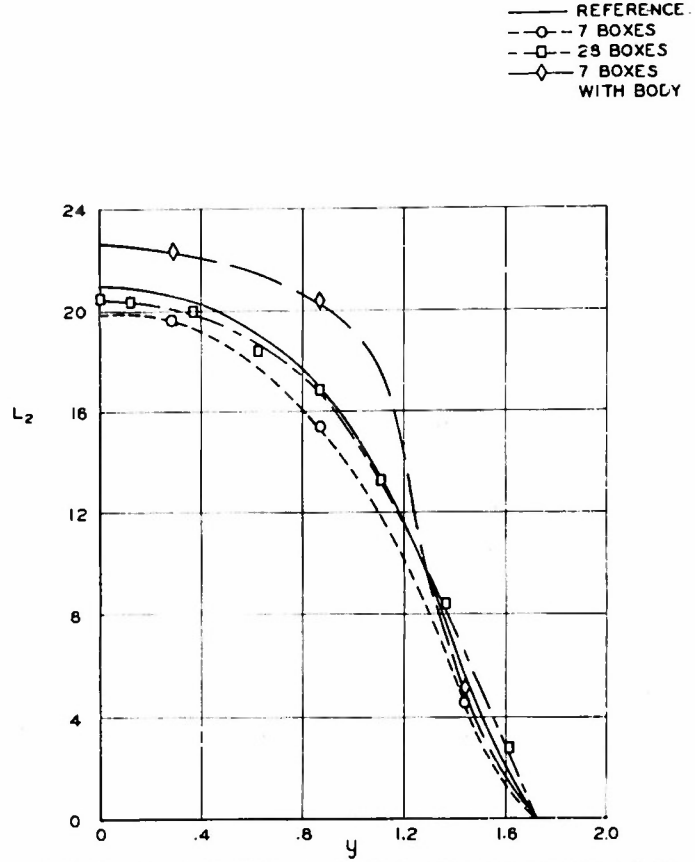

FIGURE 4. SPANWISE VARIATION OF IMAGINARY PART OF LIFT DUE TO TRANSLATION, L_2

$x_0 = 2.25$ $M^2 = 1.75$ $K = .04$ DIAMETER = .25 SPAN

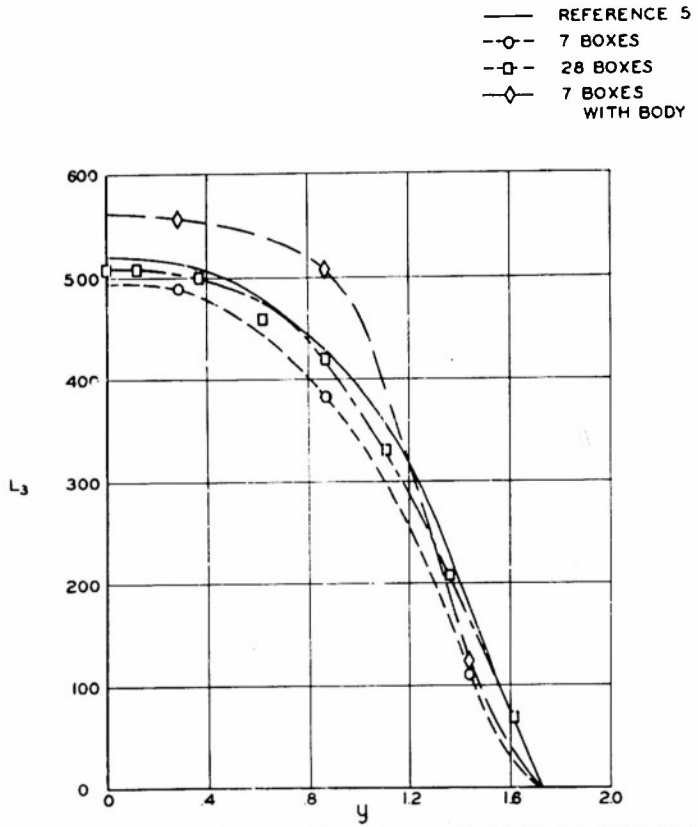

FIGURE 5. SPANWISE VARIATION OF REAL PART OF LIFT DUE TO PITCHING ABOUT ROOT MIDCHORD AXIS, L_3

x_o = 2.25 M^* = 1.75 κ = .04 DIAMETER = .25 SPAN

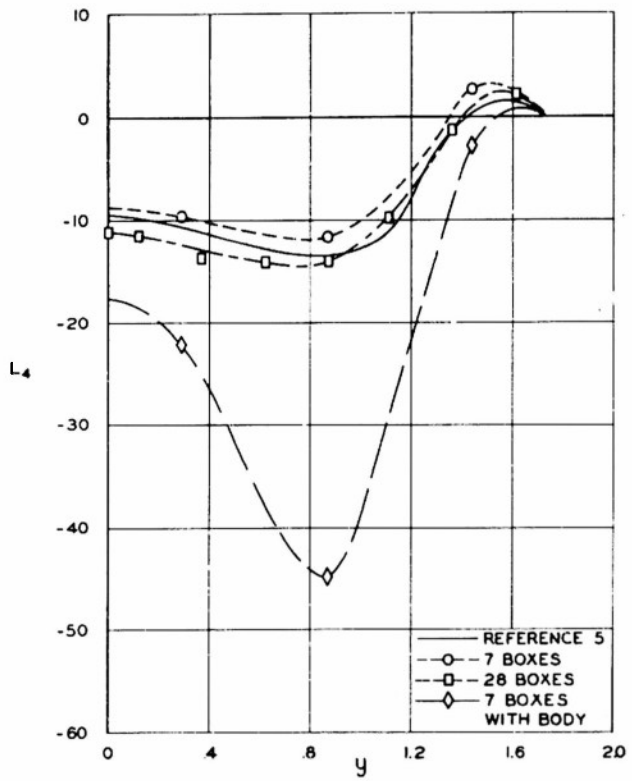

FIGURE 6. SPANWISE VARIATION OF IMAGINARY PART OF LIFT DUE TO PITCHING ABOUT ROOT MIDCHORD AXIS, L_4

x_o = 2.25 M^* = 1.75 κ = .04 DIAMETER = .25 SPAN

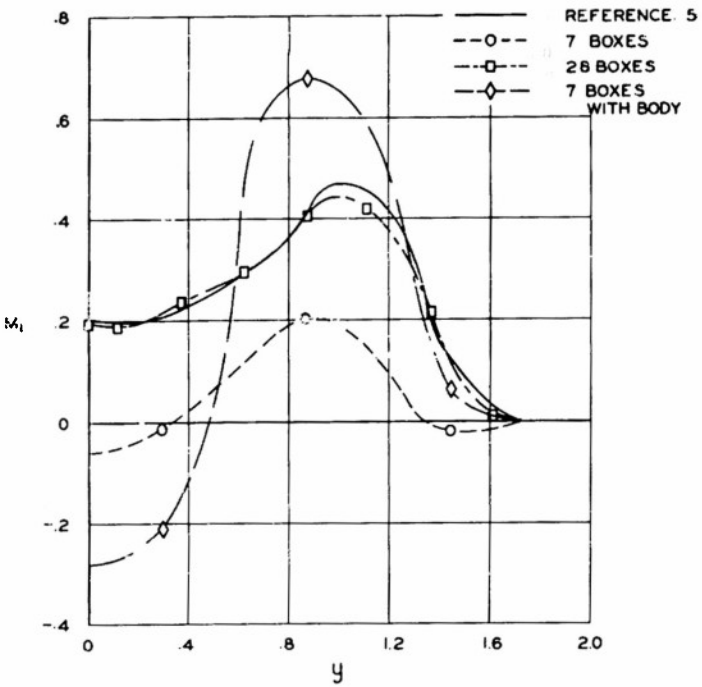

FIGURE 7. SPANWISE VARIATION OF REAL PART OF MOMENT DUE TO TRANSLATION, M_1
$x_0 = 2.25$, $M^2 = 1.75$ $K = .04$ DIAMETER = .25 SPAN

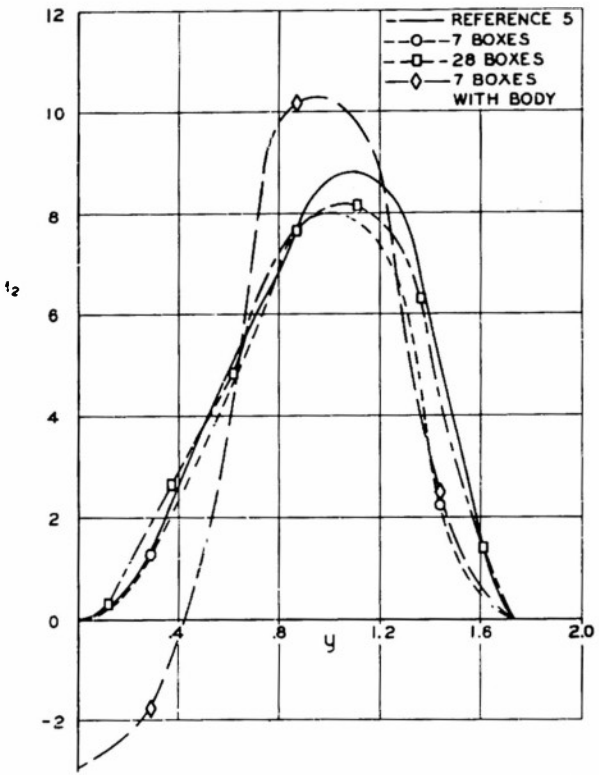

FIGURE 8. SPANWISE VARIATION OF IMAGINARY PART OF MOMENT DUE TO TRANSLATION, M_2
$x_0 = 2.25$ $M^2 = 1.75$ $K = .04$ DIAMETER = .25 SPAN

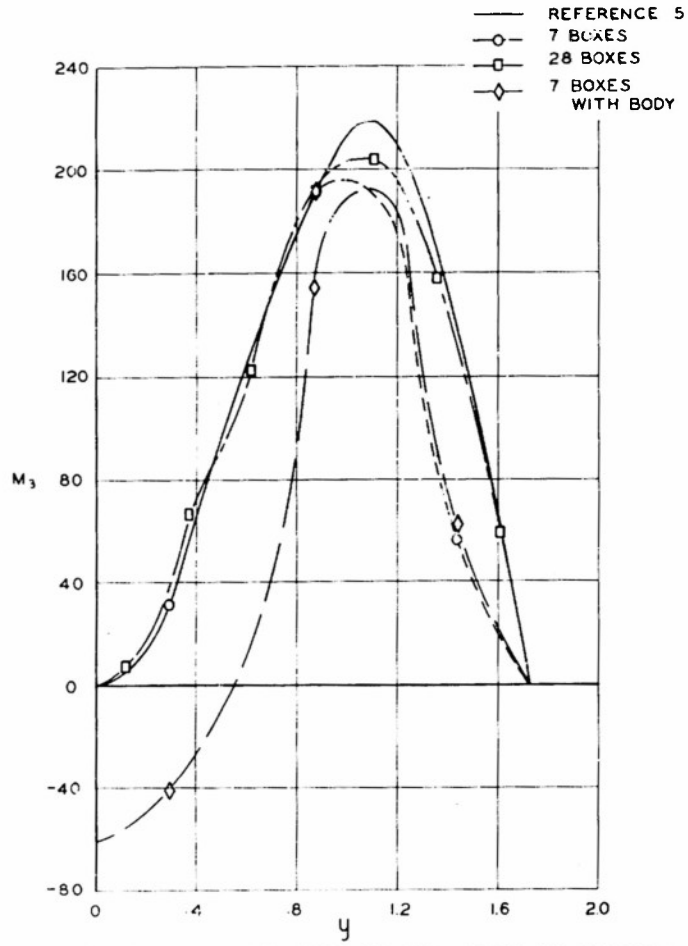

FIGURE 9. SPANWISE VARIATION OF REAL PART OF MOMENT DUE TO PITCHING ABOUT ROOT MIDCHORD AXIS, M_3

$x_o = 2.25$ $M^2 = 1.75$ $K = .04$ DIAMETER = .25 SPAN

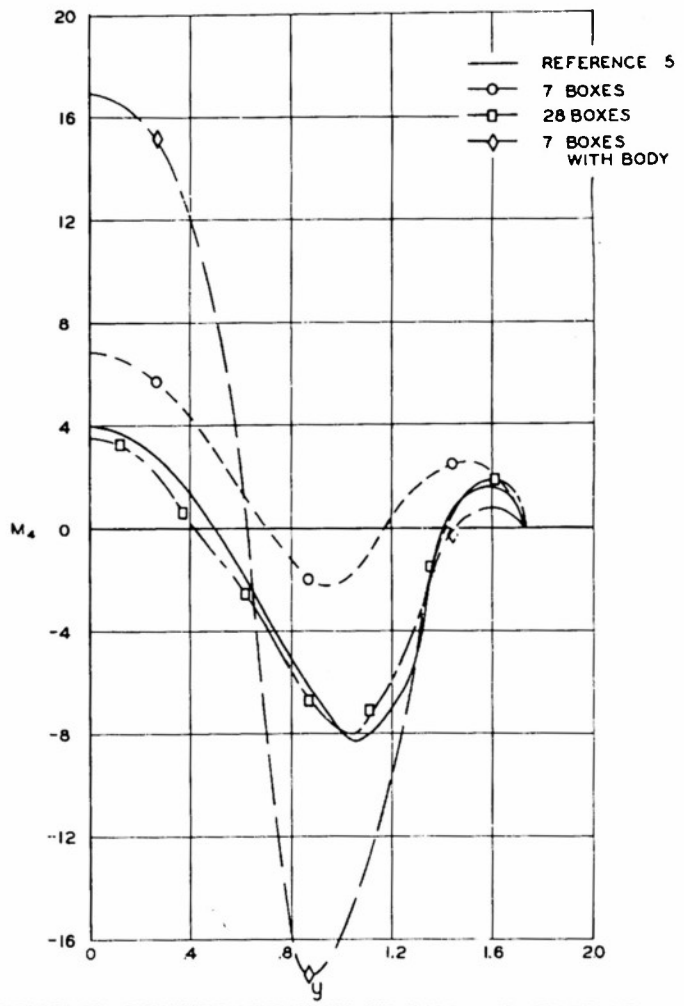

FIGURE 10. SPANWISE VARIATION OF IMAGINARY PART OF MOMENT DUE TO PITCHING ABOUT ROOT MIDCHORD AXIS, M_4

$x_o = 2.25$ $M^2 = 1.75$ $K = .04$ DIAMETER = .25 SPAN

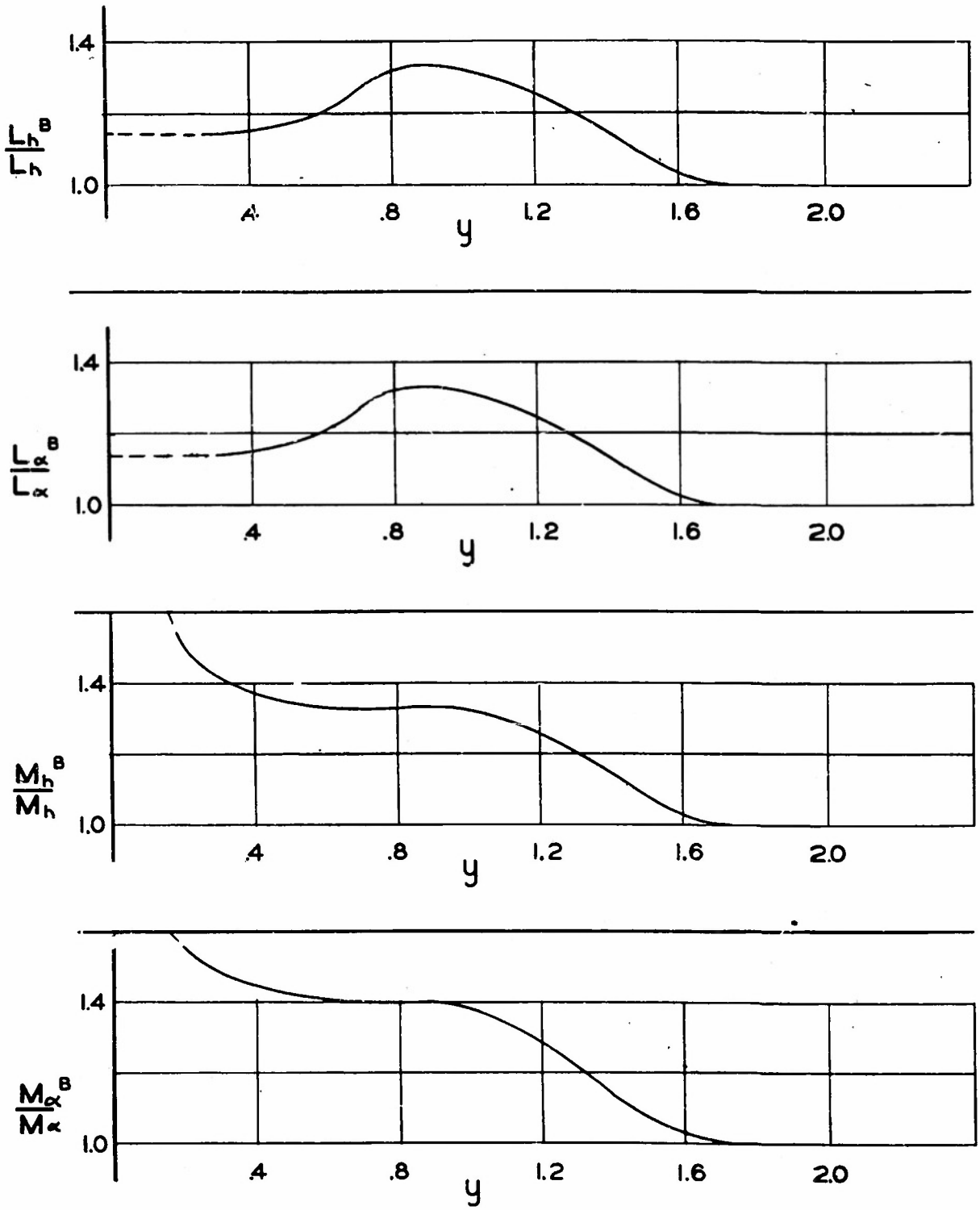

FIGURE 11. SPANWISE VARIATION RATIO OF LOAD WITH BODY TO LOAD WITHOUT BODY

$x_o = 2.25$, $M^2 = 1.75$, $\kappa = .04$ DIAMETER = .25 SPAN

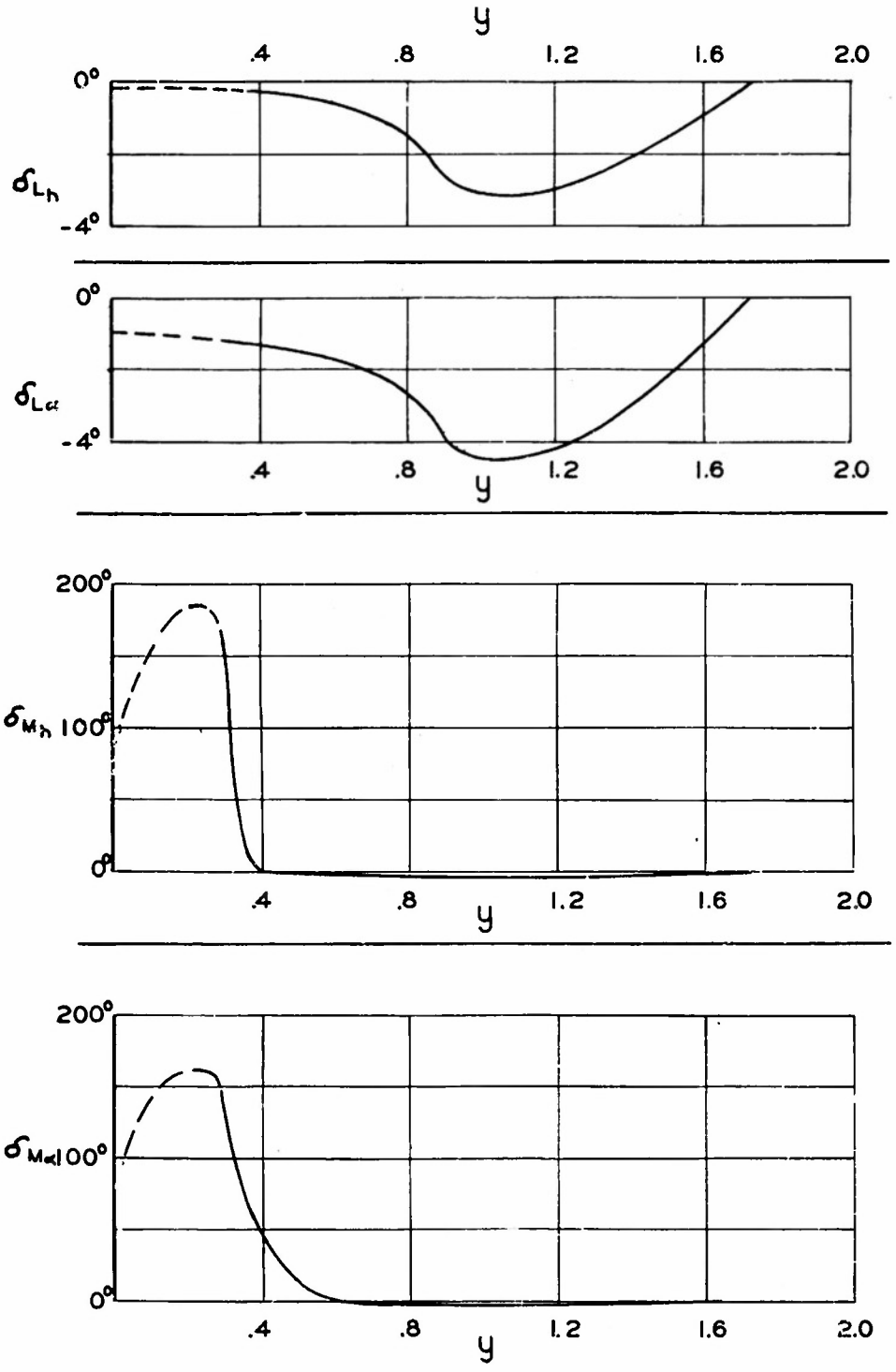

FIGURE 12. SPANWISE VARIATION OF PHASE SHIFT DUE TO ADDING BODY

$x_o = 2.25$ $M^2 = 1.75$ $\kappa = .04$ DIAMETER = .25 SPAN